RESEARCH ARTICLE | JUNE 18 2013

Jamming and shear for granular materials FREE

R. P. Behringer; Joshua Dijksman; Jie Ren; Jie Zhang; Trushant Majmudar; Bulbul Chakraborty; Daipeng Bi; Antoinette Tordesillas

AIP Conf. Proc. 1542, 12–19 (2013)
https://doi.org/10.1063/1.4811860

Jamming and Shear for Granular Materials

R. P. Behringer, Joshua Dijksman, Jie Ren, Jie Zhang*, Trushant Majmudar**[*], Bulbul Chakraborty, Daipeng Bi***[†] and Antoinette Tordesillas[**]

[*]*Duke University, Durham, NC 27708, USA*
[†]*Brandeis University, Waltham, MA 02453, USA*
[**]*University of Melbourne, VIC 3010, Australia*

Abstract. This paper describes a series of experiments which have explored systems of frictional disks that have been prepared near jamming and then subjected to shear strain. A key observation is that below a density (described by packing fraction, ϕ) of about $\phi_J \simeq 0.84$, it is possible to prepare stress-free states, and then by applying shear, traverse states that are fragile (highly anisotropic), shear jammed, and then increasingly isotropic. The anisotropy of these states is a dominante feature in the shear jamming process, which differs from the Liu-Nagel scenario. The evolution of these states suggests that an activated process in the context of a force (or stress) ensemble characterizes the stress evolution during cyclic strain.

Keywords: Shear jamming, force networks, activated processes
PACS: 45.7-.-n, 83.80.Fg, 87.57.N-

INTRODUCTION

The way in which particulate systems transition from fluid-like to solid-like is expected to depend on a number of parameters[1, 2, 3, 4, 5, 6]. Density is foremost among these, since high-density packings with many contacts cannot flow, and low-density packings with few or no contacts cannot be rigid. Often, the density is expressed in terms of the packing fraction, ϕ. However, density alone may not control this jamming transition. For instance, temperature, T, may also be important for systems such as glasses and colloids. In general, a particulate system can also be made to flow under sufficiently large shear stress, τ. In addition, shape and friction play key roles for granular systems.

Liu and Nagel suggested a scenario[1] that encapsulates these basic concepts and that might apply for many different particulate systems. The key idea was that qualitatively different systems might exhibit common jamming properties in a phase space spanning τ, ϕ, and T. For systems of macroscopic granular particles with dissipative interactions, T is not a relevant variable, and the Liu-Nagle jamming diagram reduces to the $\tau - \phi$ plane, as in Fig. 1a. In this picture, to the right of the solid slanting yield stress curve, states are jammed, and to the left unjammed. There is a special point, ϕ_J, which is thought to be critical. Below ϕ_J, there are no jammed states; above ϕ_J, states with $\tau = 0$ are jammed. However, it is possible to cause a state with $\phi > \phi_J$ to flow by applying a large enough shear stress. The locus of points along which such flow can just begin is the yield stress curve, which is the slanting curve that separates unjammed and jammed states. In the limit that τ vanishes, the yield stress curve terminates at point J. The Liu-Nagel diagram has been explored by extensive studies based on frictionless disks and spheres.[8, 4]

Recently, Bi et al., Zhang et al.[5, 9] and Ren et al.[6]have shown that for frictional granular systems, a richer set of phenomena occur in the $\tau - \phi$ plane (i.e. for $T = 0$), which we sketch in Fig. 1b. As in the Liu-Nagel scenario, for $\phi > \phi_J$, there are no unjammed states for $\tau = 0$. But, there exists a range of ϕ below ϕ_J, $\phi_S < \phi < \phi_J$, for which there are unjammed (i.e. totally stress-free) states which can be caused to jam by applying shear strain, without any change of volume (area in 2D). Starting from a stress-free state in $\phi_S < \phi < \phi_J$, the application of shear strain causes a) first, a highly anisotropic fragile state characterized by long force chains in the compressive direction, b) then a jammed anisotropic state (shear jammed), and then c) gradually more isotropic states. Note that, pure shear strain contracts a 2D system along one direction, expands it in the other, all the while maintaining the area constant, as sketched in Fig. 2. The compressive and dilational directions are key to the process of 'shear jamming'. Simple shear strain, which transforms a rectangle into a parallelogram, again without area change, also has compressive and dilational directions, plus rotation.

EXPERIMENTAL TECHNIQUES

Recent experiments at Duke University were carried out using systems of frictional photoelastic particles, and with various novel devices that can shear or otherwise strain samples of these particles. The use of photoelastic particles offer what is currently the unique capability of

Powders and Grains 2013
AIP Conf. Proc. 1542, 12-19 (2013); doi: 10.1063/1.4811860

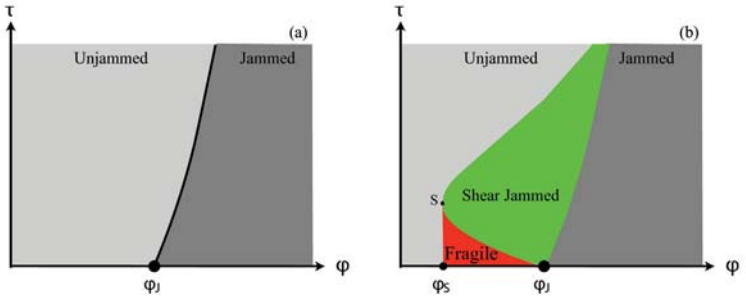

FIGURE 1. Jamming diagrams for particular materials. (a) Jamming diagram proposed by Liu and Nagel. (b) Jamming diagram obtained by Bi et al. for frictional particles.

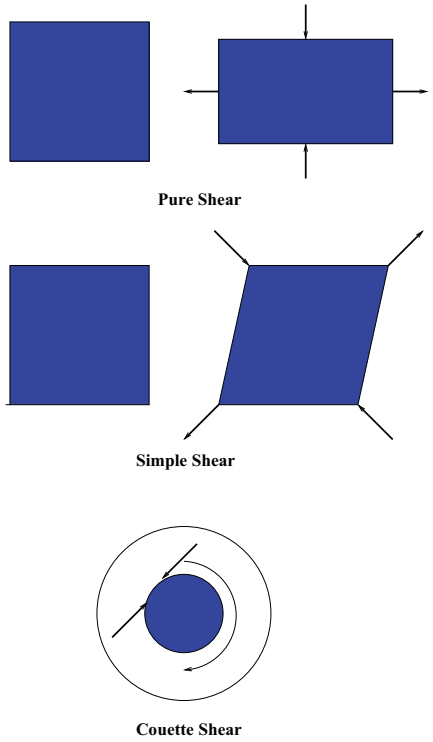

FIGURE 2. Sketch of different common ways to produce shear strain in two dimensions. Pure shear consists of compression in one direction, and dilation in the other. Simple shear strain involves is achieved by deforming a square into a parallagram, with no change of area. In this case, there is, as for pure shear, compression and dilation directions, plus rotation. A third commeon way to achieve large amplitude shear strain involves a Couette geometry.

obtaining complete vector kinematic and force information at the grain scale. We obtain three types of images, as shown in Fig. 3. For one image, the system is sandwiched between crossed polarizers, the second omits the polarizers, and the third uses UV illumination to track small fluorescent bars that are marked on each disk. Under normal illumination, these stripes are invisible, but under UV light, they glow strongly, and it is easy to track the rotation of each particle from before to after a small strain step by measuring the rotations of its bar. We obtain displacement data by well established particle tracking techniques[7]. We obtain force information from the photoelastic response of the particles, as visualized through crossed circular polarizers. There are several key steps to this process. First, we assume that the contacts are essentially point-like, i.e. that the deformation of a particle at the contact with a neighbor is much smaller than its radius. This means that the stresses within each disk can be described by a relatively simple closed-form solution in which the vector contact forces each contribute an effectively additive point-like term to the total stress field, and the stress at the edge of the disk vanishes except at the contacts. Near a contact, this solution has a $1/r$ singularity. Second, if the contact forces, F_i, are known, then the resulting photoelastic response for a ray that travels along the axial direction of a disk is also known and has the form

$$I = I_o \sin^2[C(\sigma_2 - \sigma_1)H/(\pi\lambda)] \qquad (1)$$

Here, the σ_i are the principle stresses in the plane of the disk, C, the stress-optic coefficient, is a property of the material from which the disks are made, H is the thickness of the disk, and λ is the wavelength of light used to illuminate the disk with incident intensity, I_o. Third, we now determine the contact forces by solving the inverse problem for the vector forces that yield a given photoelastic pattern within the disk. Note that this process is aided by the fact that the contacts are known, first by determining proximity of particles, and second by the fact that even very weak contacts show a photoelastic

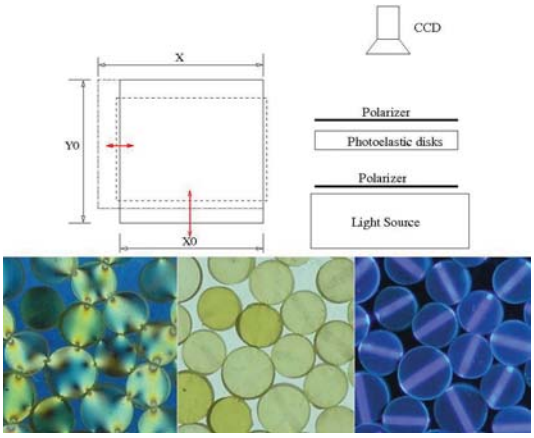

FIGURE 3. Biaxial experiment. Top left: sketch of functionality of the biaxial apparatus; Top right: sketch showing a side view of the imaging technique used to produce photolelastic images. Bottom row shows cropped images for, left to right, polarized image, unpolarized image, and UV-illuminated image.

response due to the $1/r$ effect in the stress. For any given photoelastic image of a particle subject to a finite number of point forces with force and torque balance, there is a unique set of forces that yield that pattern.

We have used several different approaches to apply strain to our photoelastic systems, and I will describe them briefly here. Our first apparatus, a kind of biaxial tester, as sketched in Fig. 3, allows us to apply independent strains in each of two orthogonal directions, e.g. say the x and y directions. The particles within this apparatus rest on a smooth, horizontal, powder-lubricated Plexiglas sheet, and the two strains can be applied in this plane by moving opposing pairs of walls. Thus, we can apply isotropic compression by equal relative contraction of both dimensions of the system. We apply shear strain by contracting one dimension while expanding the other, keeping the system area constant. And, we can also apply any combination of contraction/expansion of the two sets of walls. A second approach that is described more fully in a separate paper in this proceedings and elsewhere[6], is a simple shear apparatus that has the special property that the base deforms in concert with the walls. Thus, instead of applying the shear just from the boundaries, we apply shear strain that acts everywhere in the system. The result is a system that remains free of unwanted inhomogeneities, such as shear bands, even for many shear cycles. A third experimental approach[10], discussed elsewhere in this proceedings, elliminates the friction between the Plexiglas base and the particle altogether. This is achieved with a simple shear apparatus (driven just from the walls) where the particles are also floated in a layer of fluid, water plus salt, that has a density that is just slightly greater than that of the particles.

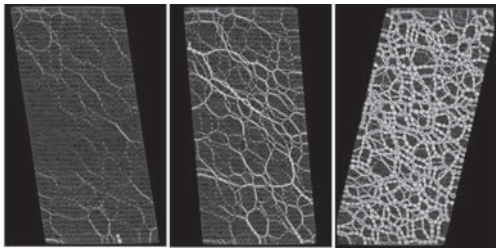

FIGURE 4. Photoelastic images show from left to right: a state that is close to the transition to a fragile state; a state that is close to shear jammed, and a more nearly isotropic state that is strongly jammed. In the fragile state, the strong force network percolates in the compressive direction only; in the shear jammed state, the strong force network percolates in all directions.

A fourth Couette apparatus[11] shears a horizontal layer of particles between an inner rotating wheel and an outer fixed ring. Although there is inadequate room to discuss all of the results from these experiments, it is important to emphasize that they all show shear jamming of frictional disks[12, 9, 5, 6].

THE NATURE OF THE SHEAR JAMMED STATE

We next consider what happens in the shear jamming regime. Starting from a stress-free state, the application of increasing amounts of shear strain first produces a 'fragile' state[2], then ultimately, a jammed state. Fig. 4 shows examples of the photoelastic images that span the range from fragile to shear jammed, to strongly jammed. The fragile state is characterized by highly anisotropic force and contact networks that percolate from one boundary to the other in the compressive direction, but that do not percolate in the dilation direction. This is similar to what was envisioned by Cates et al.[2] for colloidal systems. If the system is sheared past the fragile regime, shear jamming occurs when force and contact networks percolate in both directions. If additional shear strain is applied, past the point of shear jamming, then the system tends to become more isotropic. For instance, the shear stress peaks and may actually decrease for large enough shear strain.

Conventional fabric and stress tensors provide important characterizations of these states. If a particle has N contacts, with forces, $\vec{F}_i$, acting at branch vectors $\vec{r}_i$, then the fabric tensor associated with that particle is the diadic product of the unit normals of the branch vectors, summed over all contacts, as in Eq. 2. The stress is the diadic product of the branch vectors with the corresponding contact forces, all normalized by the area associated with the particle. The branch vectors are the vectors from the center of mass of the particle to the corresponding

contact. Continuum fabric and stress tensors then follow from an appropriate coarse graining. (For a discussion of coarse graining approaches, see Goldenberg and Goldhirsch[13].) An important question is then how to select a coarse graining scale. We construct the stress tensor and an averaged contact fabric tensor $\hat{R}$ for the system by summing:

$$\hat{\sigma} = \frac{1}{V}\sum_{i\neq j}\vec{r}_{ij}\otimes\vec{f}_{ij},$$
$$\hat{R} = \frac{1}{N}\sum_{i\neq j}\frac{\vec{r}_{ij}}{\|\vec{r}_{ij}\|}\otimes\frac{\vec{r}_{ij}}{\|\vec{r}_{ij}\|}, \tag{2}$$

An important aspect of the states considered here is that the grains, and in particular the connected grain networks, 'carry force' from one boundary to another. In that case, the connectedness (and other topological properties) of the force networks are important[14]. The idea of force networks draws from the well established idea of force chains[15, 16]. A useful concept is to consider networks of connected particles that experience a mean normal force in a given range. Refering to Eq. 2, the mean normal force acting on a particle corresponds to the particle scale 'pressure' where quotes are used here, since the pressure conventionally refers to a coarse grained quantity. Then, heuristically, force chains are connected particles that have above average local pressure. Fragile states, as in Fig. 4-left have force chains that percolate only between in the compressive strain direction. Shear jammed states, e.g. Fig. 4–middle and right, have force chains that percolate in all directions. In particular, Fig. 4–middle is close to the onset of shear jamming. And Fig. 4-right shows that the application of shear strain past shear jamming produces more isotropic states.

Anisotropy is key to the fragile and shear jammed states. For instance, states that are characterized by long force chains in only one direction, such as the fragile states, have a highly anisotropic stress and fabric tensors. In Fig. 5, we show explicitly that the cluster size of the percolating fabric grows with increasing strain first in the compressive direction, and then later, in the dilational direction. Here the largest cluster of the fabric is indicated in green (from Bi et al.[5]).

We then collect all such data and present them in Fig. 6. In this figure, states that are unjammed are indicated by a black dot, those that are in a fragile state by a red dot, and those that are completely jammed by a gree dot. The solid (purple) line is an estimate of the yield stress curve.

The density range for shear jamming is limited, and occurs for $\phi_S \leq \phi \leq \phi_J$, as shown in Fig. 7. This range is set by two constraints. First, above ϕ_J, states with $\tau = 0$ have $P \neq 0$ and are isotropically jammed, as in the original Liu-Nagle scenario. Below ϕ_S, the particles are far enough apart that no amount of shear strain will cause

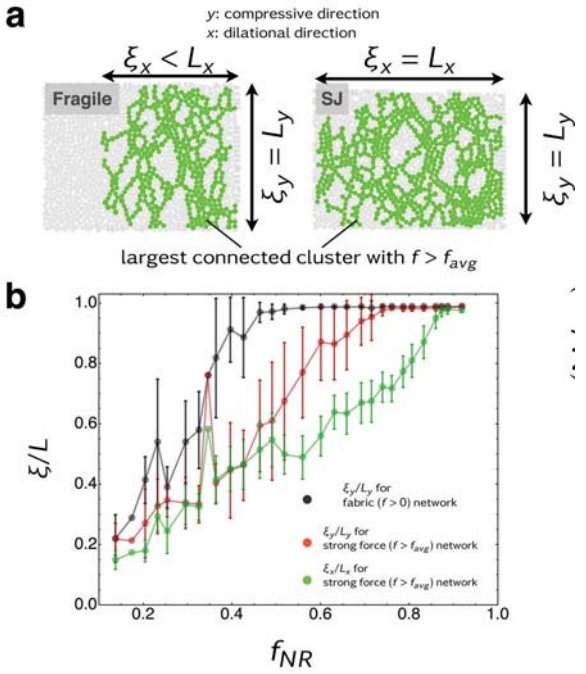

FIGURE 5. Force networks (from Bi et al.[5] from biaxial experiments). (a) Left: Typical fragile state–the strong force network percolates in the compressive direction but not the dilational direction; Right: shear jammed states–the strong force network percolated in all directions. The linear sizes associated with the largest connected cluster in the strong force networ are ξ_x and ξ_y. Lx and Ly are box dimensions. (b) Cluster size normalized by box dimensions dimension vs. the non-rattler fraction $f_N R$ for the fabric and the strong force network. Black: fabric in the compressive direction; Red: strong force network in the compression direction; Green: strong force network in the dilation direction and the compressive direction. All data are represented as mean plus standard deviation.

jamming. Note that the amount of shear strain needed to reach shear jamming appears to diverge from above at ϕ_S.

RESPONSE AND DYNAMICS NEAR SHEAR JAMMING

The above characterization of shear jamming raises a number of questions. For instance, what is the generalized elastic response near shear jamming? What, if any, connection is there between shear jamming, and isotropic jamming that occurs near $\phi \simeq 0.84$ for unsheared systems[17]? If the system is subject to repeated shear, is there any systematic evolution? What particle-scale processes occur during shear jamming? This section addresses a number of these questions, which have also been discussed by Ren et al.[6]. In order to probe most of these issues, it is important to have an ex-

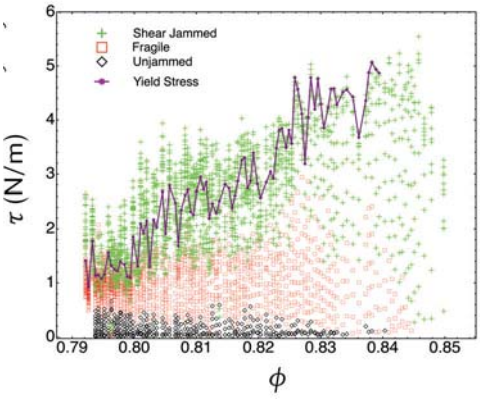

FIGURE 6. Jamming diagram (from Bi et al.[5] from biaxial experiments). Experimentally determined states in the $\tau - \phi$ plane. Red, green and black points, corresponding respectively to fragile, shear jammed, and non-percolating networks, defined by the criterion of force network percolation in part (b) or the previous figure. Purple line: Estimated yield stress line.

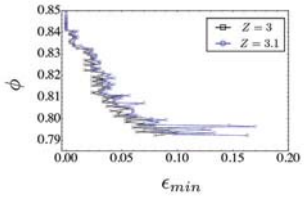

FIGURE 7. Minimum strain to shear jamming vs. ϕ. At $\phi_J \simeq 0.84$, no shear strain is need to jam, and at higher densities, the system is jammed at $\tau = 0$. At a lowest density, $\phi_S \simeq 0.79$ (in these experiments), it was not possible to apply shear strain and arrive at a shear jammed state.

perimental system that provides shear strain uniformly across the system, so that any response is characteristic of the whole system, and not simply some part. In order to have such a system, we developed the apparatus, discussed above in the context of simple shear, and in Ren et al.[6]. This apparatus applies simple shear strain uniformly across a quasi-2D system of bidisperse disks. The apparatus can apply strains of up to roughly $\pm 25\%$. We then carried out two related types of experiments with this device. In one type of experiment, we applied shear strain uniformly up to some peak value, γ_{max}. In the second type of experiment, we carried out shear cycles, in which the system was sheared between two strain values, $\gamma_{min} < \gamma_{max}$. We will distinguish symmetric shear, for which $\gamma_{min} + \gamma_{max} = 0$, and non-symmetric shear for which this quantity is non-zero.

We first demonstrate that the apparatus does indeed provide close to uniform shear throughout. In Fig. 8, we show the displacements for the particles, following a uni-directional shear strain of 27%, in part (c) of the figure. Here, the y-direction corresponds to the 'moving' direction in which the shear strain is applied. The y-displacements of the particles then match to the applied affine strain provided by the apparatus. Note that the x-positions of the particles are largely unchanged as the result of shear strain. Part (d) of the figure shows the coarse grained density of the system after 27% shear strain. Although there are random fluctuations in the density, as expected, there are no systematic density gradients, such as those that would occur during shear banding.

We next address the issue of generalized elastic response. We begin by considering first the pressure as a function of shear strain. Note that the process of shear jamming creates states for which the pressure, $P = (\sigma_1 + \sigma_2)/2$ and $\tau = (\sigma_2 - \sigma_1)/2$ are non-zero. Here, the σ_i are the system-wide principal stresses, i.e. the eigenvalues of the stress tensor. Necessarily, $P \geq \tau$, where equality occurs only in the extreme fragile limit where one of the principal stresses vanishes. Since P grows in response to shear strain, and it cannot be sensitive to the (initial) choice of shear strain direction, we expect that P will be an even function of strain. In fact, to a reasonable approximation, we find that P is an even function of strain, for uni-direction shear strain experiments, as shown in Fig. 9. We can fit the data to $P = (R/2)\gamma^2$, which then defines the 'Reynolds coefficient', $R = \partial^2 P(\gamma)/\partial\gamma^2$. We coin the name Reynolds coefficient because the $P - \gamma$ relation is reminscent of more conventional Reynold's dilatancy, which occurs when a system expands when it is sheared. Of course, the effect observed here differs from the more conventional effect on several counts. First, the usual Reynold's dilatancy occurs for a jammed system, unlike the present case. And, second, the conventional effect leads to an increase in volume (perhaps at constant P), whereas here, the volume is fixed, so that the response occurs as in increase in pressure.

It is then an interesting investigate the dependence of R on relevant parameters. First, note that the data of Fig. 9 indicate that R does not depend on γ. By inference, it must depend only on ϕ, and indeed, as shown in Fig. 9(b), it it exhibits power-law behavior, with a strong divergence: $R = A(\phi_c - \phi)^\alpha$, where A and α are constants. The divergence of R at ϕ_c is strong: $\alpha = -3.3 \pm 0.1$. And, particularly intriguing is the fact that $\phi_c = 0.841 \pm 0.004$, i.e. indistinguishable from the isotropic shear jamming density seen by Majmudar et al.[17].

During the shear strain that leads to jamming, there are always small particle displacements, and concomitant evolution of the force networks. In particular, these

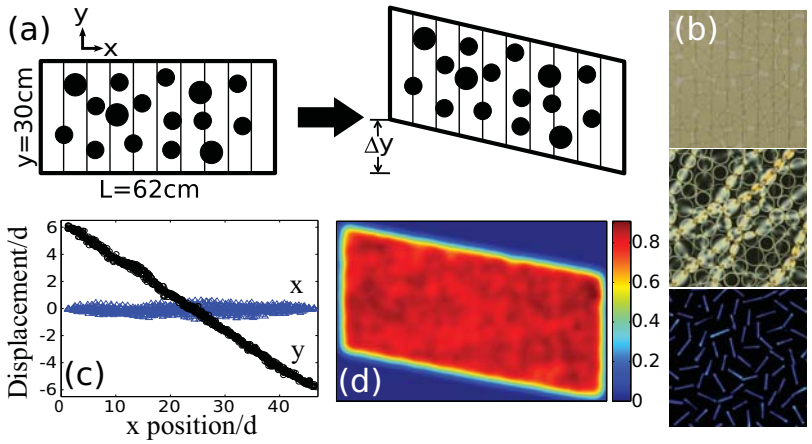

FIGURE 8. (a) Sketch of functionality of simple shear apparatus; (b) small portions of images without/with polarizers and with UV light; (c) displacements of particles for a strain of 27%; (d) false color map of locally coarse grained density, after the same shear of 27%.

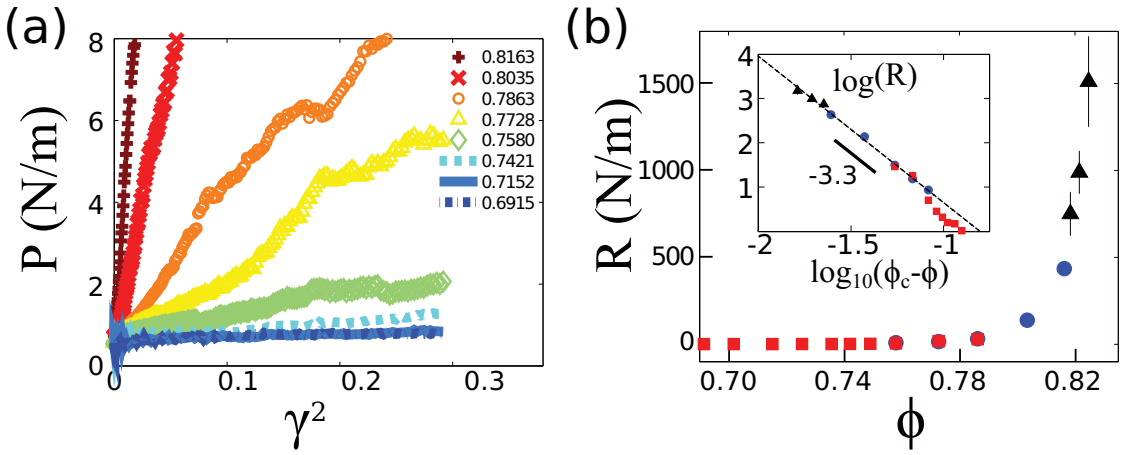

FIGURE 9. Pressure vs. γ^2 and the Reynolds coefficient, R as a function of ϕ.

changes do not seem to ever be reversible when the shear deformation is reversed. This raises the last question that we address here: is there any long term evolution of the system under cyclic shear, and if so what is the nature of the evolution and the associated fluctuations? To at least partially address this issue, we carried out a series of cyclic shear runs, as noted above. Each run started from an unjammed state. We then characterized the system-averaged stress over many cycles. Fig. 10 (a) shows that the global P is nearly reversible if the strain is symmetric: $\gamma_{min} + \gamma_{max} = 0$. In this figure, we show only a few of the cycles to emphasize the fact that after a very modest initial transient, P followed a similar path as a function of γ. Note, however, that the shear stress, τ, shown for the same symmetric set of cycles in Fig. 10, is not at all reversible, and shows substantial hysteresis. This hysteresis is an immediate consequence of the fact that the major principal stress eigen-direction changes in response to changes in the shear direction. But because the system actually shear jams, τ does not drop to zero on reversal of the strain. Perhaps more surprising is the system response to non-symmetric shear. In part (c) of Fig. 10, we show the evolution of the system pressure for the case where $\gamma_{min} = 0$ and $\gamma_{max} = 0.045$. For the early cycles, P is not at all symmetric in γ. But, with with increasing cycle number, the system $P(\gamma)$ (unlike τ)approaches a reversible symmetric path. That is, the force and contact networks within the system slowly evolve towards an attractor, such that $P(\gamma)$ is symmetric about the mid-point between the two extremes of shear strain. A simple measure of the evolution towards a symmetric $P-\gamma$ curve is $\Delta P(n) = P(\gamma_{max}) - P(\gamma_{min})$, where n is the cycle number. We show data for ΔP vs. n in Fig. 11(a). For all cases, ΔP evolves as the logarithm of n, and it is possible to fit each relaxation curve to the form $\Delta P(n) = \beta \log(n/n_o)$, where n_o is a natural 'time scale' for the relaxation. Data for ΔP vs. n/n_o, in Fig. 10(b) show a very striking collapse: all data for a given strain amplitude, γ_A, collapse onto a common curve, with a common value of $\beta(\gamma_A)$, regardless of the density. It follows that a complete collapse of all the data occurs for $\Delta P/\beta(\gamma_A)$ vs. n/n_o. The logarithmic relaxation is then strongly suggestive of an activated process. In the present case, the evolution is stress-controlled, suggesting a connection to a stress ensemble description[18].

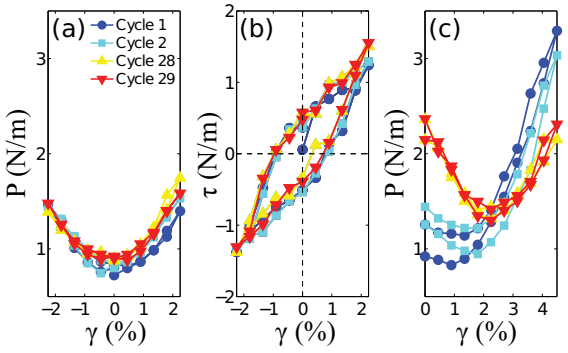

FIGURE 10. Cycles of pressure and shear stress, as discussed in the text.

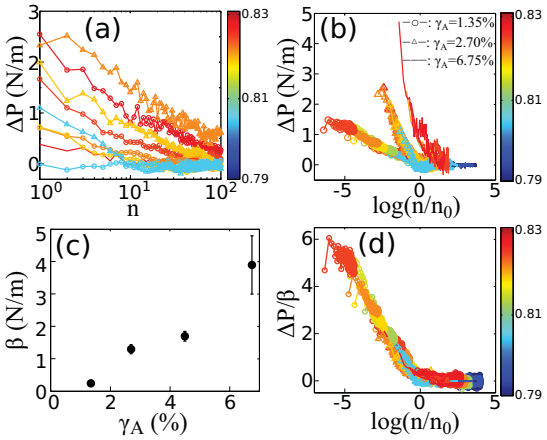

FIGURE 11. Logarithmic evolution of $\Delta P(n)$, as discussed in the text.

CONCLUSIONS

The present paper has outlined some of the basic features of the transitions to fragile and shear jammed states, as obtained through experiments and analysis of quasi-2D systems of frictional disks. However, there remain a significant number of open questions. The experiments to date have shown shear jamming for particles that have static friction coefficients of about $\mu_s = 0.6$. The role of friction between particles is not yet clear. For instance, interparticle friction can help stabilize force chains, which would support shear jamming. But, recent simulations indicate that shear jamming can occur for frictionless particles[19, 20]. The details of local processes, and the connection between force/contact networks and particle kinematics are still an open question. And, the the data of Ren et al.[6] suggest an intriguing possibility that the states of shear jammed systems are controlled by activated processes for states in a force ensemble.

ACKNOWLEDGMENTS

We appreciate many helpful conversations with Corey O'Hern, Martin van Hecke, and Lou Kondic. Work supported by NSF grants DMR-0906908, DMR-1206351, ARO grant W911NF-11-1-0110, and NASA grant NNX10AU01G. .

REFERENCES

1. A. J. Liu and S. R. Nagel, Nature **396**, 21 (1998).
2. M. E. Cates J. P. Wittmer J.-P. Bouchaud and P. Claudin, Phys. Rev. Lett. **81**, 1841 (1998).
3. Bulbul Chakraborty and R. P. Behringer, Jamming of granular matter, in Encyclopedia of Complexity and System Science, Springer, **39**, 4997-5021 (2009).
4. M. van Hecke, J. Phys. Condens. Matter**22** 033101 (2010).
5. Dapeng Bi, Jie Zhang, Bulbul Chakraborty, and R. P. Behringer, Nature **480** 355-358 (2011).
6. Jie Ren, Joshua A. Dijksman and R. P. Behringer, Phys. Rev. Lett. **110**, 018302 (2013).
7. T. Peng, A. Balijepalli, S. K. Gupta, T. LeBrun, J. Comput. Inf. Sci. Eng. **7** 330 (2007).
8. C. S. O'Hern, L. E. Silbert, A. J. Liu and S. A. Langer, Phys. Rev. E **68**, 011306 (2003).
9. J. Zhang, S. Majmudar, A. Tordesillas and R.P. Behringer, Granular Matter **12** 159 (2010).
10. H. Zheng, J. Dijksman and R. P. Behringer, to be published.
11. S. Farhadi and R. P. Behringer, to be published.
12. D. Howell, R. P. Behringer, & C. Veje, Phys. Rev. Lett., **82**, 5241-5244, (1999).
13. C. Goldenberg ad I. Goldhirsch, Continuum Mechanics for Small Systems and Fine Resolutions, pp. 1-58, in Handbook of Theoretical and Computational Nanotechnology, M. Rieth and W. Schommers, eds., American Scientific Publishers, (2005).
14. M. Kramer, L. Kondic and K. Mischaikov, private communication.
15. F. Radjai and D. Wolf and S. Roux and M. Jean and J. J. Moreau, in Friction, Arching and Contact Dynamics, D. E. Wolf and P. Grassberger, World Scientific, Singapore, 1997.
16. Y. Zhang and P. A. Cundall, Proc. Symp. on the Mech. of Particulate Media 10th National Congress on Applied Mechanics, (1986).
17. T. S. Majmudar, M. Sperl, S. Luding and R. P. Behringer, Phys. Rev. Lett. **98** 058001 (2007).
18. S. F. Edwards and R. B. S. Oakeshott, Physica D **38**, 88 (1989).
19. N. Kumar and S. Luding, preprint (2012).
20. C. O'Hern, private communication.